Theorization and Modeling Ⅲ
(Review)

Modeling of EML in Combined AC/DC Magnetic Fields as the Basis for Microgravity Experiments

Koulis PERICLEOUS, Valdis BOJAREVICS and Alan ROY

Abstract

This article contains a review of research activity in the University of Greenwich to model the effects of static or DC magnetic fields on the characteristics of EM-levitated melts. The general idea is that the presence of a DC field will damp out the velocities inside a levitated droplet and so lead to more accurate thermophysical property measurements, especially those of viscosity and thermal conductivity that will otherwise be affected by turbulence. The technique is in fact used successfully in terrestrial experiments, and this study sets out to examine its applicability in the case of microgravity. An accurate spectral-collocation numerical scheme is used to couple dynamically the velocity, temperature and magnetic fields, so that internal velocity and liquid envelop changes of a suspended "spherical" droplet can be observed as a function of applied AC and DC fields, with or without gravity.

1. Introduction

Since the earliest Electro Magnetic (EM) levitation experiments in AC magnetic field[1] it became apparent that the levitated liquid metal is prone to oscillation and instability. Both EM and electrostatic (ES) levitation experiments with liquid metal droplets show difficulties related to confinement stability and a need for complex correction functions to establish a correlation between the measurements and the droplet material properties[2,3]. Intense internal fluid flow is visually observed, apparently being in the turbulent regime for earthbound conditions. This behavior was also observed in numerical simulations[4,5].

In addition to metrology, and usually on a larger scale, there is demand for melting reactive materials without contamination, for example titanium alloys for high quality castings. However, it is often difficult to achieve the required superheat in the melt with traditional 'cold' crucible-type furnaces due to a partial contact with the water cooled copper walls[6]. In this respect, it was found that a DC field acting together with the AC induction field would damp out turbulence and reduce free surface oscillations thereby increasing superheat. Applications include the evaporation of levitated melts for coating purposes or the supply of pure superheated melt for metal powder production[7]. At the other temperature extreme, a highly under-cooled liquid can be obtained before solidification to a glassy structure in the levitated conditions in absence of nucleation centers[8].

Finally, a combination of AC and DC magnetic fields is recognized as an efficient technique in stabilizing high temperature levitated melts, preventing contact to contaminating walls[9,10]. The intense AC magnetic field required to produce levitation (in full gravity), acts in a thin external region of the levitated mass (the skin layer) resulting in high shear flow and turbulent large-scale toroidal recirculation. In contrast a static magnetic field acts uniformly throughout the liquid volume resisting toroidal flow. Turbulence leads to an apparent viscosity which behaves non-linearly, and can be 2-3 orders of magnitude higher than molecular viscosity. This alters the damping rate of oscillating droplets making the measurement of viscosity very uncertain[11] and it diffuses heat much faster within the melt, making conductivity measurements impossible. The effect is non-linear and depends on the relative intensity of the DC and AC fields applied[10]. It was found, that in typical terrestrial melting conditions one can approach the laminar state for viscosity and heat transfer when the applied DC magnetic field exceeds 4-5T[9]. An electrically conducting droplet in a high DC magnetic field behaves quite differently to a non-conducting one. For example, the asymptotic solution of Priede[12] for high magnetic field, shows damping of the even axisymmetric oscillation modes, but the odd modes are not damped or are only moderately damped.

The behavior of liquid melts in a combination AC and DC field, with or without gravity is the subject of this paper. Numerical models of the flow within a levitated liquid sample, coupled with the behavior of the moving free surface give an insight to the dynamics of levitated droplets of various sizes and magnetic field intensities. Realistic gradient fields, typical of the solenoidal coils encountered in superconducting magnets, are used in modeling, to validate the mathematical model against terrestrial experiments[9,13].

Centre for Numerical Modelling and Process Analysis, University of Greenwich, London SE10 9LS
(E-mail: k.pericleous@gre.ac.uk)

56

2. Numerical Model

The numerical model (code SPHINX) uses an adaptive mesh formulation of the spectral collocation method with a Chebyshev grid used for the radial direction and Legendre nodes in the vertical direction. The model uses a coordinate transformation for the free surface, which allows the problem to be solved on a unit sphere.

2.1 Electromagnetic Force Calculation

The starting assumption for theoretical models attempting to predict the free surface behavior of EM-levitated droplets is based on the idea of an infinitely thin skin layer where the high frequency AC magnetic field penetrates. This then replaces the EM force distribution by the so-called 'magnetic pressure', acting on the free surface. Such an approximation effectively removes any dependence on the electrical conductivity of the levitated material. The skin-layer approximation was tested against direct numerical solutions[14] for typical experimental frequencies and material properties (Al, Ni, Si). The results indicate that for medium frequencies (<100 kHz) the deformation and velocity field are significantly different in a 10mm droplet compared to the asymptotic skin-layer case. For higher frequencies (>100 kHz) a relatively good correspondence for the droplet shape can be obtained. The velocity field within a levitated liquid material is controlled by the volumetric EM force distribution; it is important to understand how various approximations to this force field can be obtained from a mathematical point of view. The general expression for the EM force acting on a levitated fluid volume becomes rather complex[15] if one accounts for variable electrical conductivity and magnetic properties. For uniform properties within the liquid, the commonly used expression for the force is:

$$\mathbf{f} = \mathbf{j} \times \mathbf{B} + \chi \nabla (B^2 / 2\mu_0) \qquad (1)$$

Where, $\mathbf{j}$ is the electric current density, $\mathbf{B}$ the magnetic field, χ is the volumetric magnetic susceptibility (e.g., $\chi = -4.2 \times 10^{-6}$ for silicon which is diamagnetic) and μ_0 is the magnetic permeability of vacuum in SI units. When a combination of high frequency AC and DC magnetic fields is used, a time-average of the force over the field oscillation period τ (~ 10^{-4} - 10^{-6} s) is effective with a time scale for a levitated droplet oscillation period being 10^0 - 10^{-2} Hz. However, the oscillating part of the high frequency AC field is still present within the fluid, adding a time-dependent vibrating force at double the frequency of the applied AC, in addition to the time averaged force.

In the work presented, the electromagnetic force is computed from an integral equation representation. This has the advantage that the far field boundary conditions are not explicitly required, and the electromagnetic field can be solved only in the regions where it is needed. The electric current distribution in a moving medium of conductivity σ is then given by the magnetic vector potential $\mathbf{A}$, the magnetic field $\mathbf{B} = \nabla \times \mathbf{A}$, the electric potential φ and the fluid flow induced part $\sigma(V \times \mathbf{B})$:

$$\mathbf{j} = \sigma(-\partial_t \mathbf{A} - \nabla \varphi + V \times \mathbf{B}) = \mathbf{j}_{AC} + \mathbf{j}_v \qquad (2)$$

The $\mathbf{j}_{AC}$ part of the current is induced in the conducting medium even in the absence of velocity. The governing integral equations can be obtained from the electric current distribution in the source coils and the unknown induced currents in the liquid, related to the total magnetic field and the vector potential $\mathbf{A}$ by the Biot-Savart law[15,16]:

$$\mathbf{A}(\mathbf{r}) = \frac{\mu_0}{4\pi} \iiint_{V(\mathbf{j} \neq 0)} \frac{\mathbf{j}(\mathbf{r}')}{|\mathbf{r} - \mathbf{r}'|} d\mathbf{r}' \qquad (3)$$

Equations (2) and (3) can be solved in the axisymmetric case for harmonic fields as in[5].

The induced current in the liquid drop depends on its instantaneous free surface shape and needs to be recomputed as the shape changes during oscillation. The electromagnetic force $\mathbf{f}$, time-averaged over the AC period, can be decomposed in two parts: $\mathbf{f} = \mathbf{f}_{AC} + \mathbf{f}_v$ as in (2). The second, fluid-velocity-dependent part $\mathbf{f}_v$, can include both DC and AC time-averaged contributions. The electromagnetic force associated to the electric current $\mathbf{j} = (\nabla \times \mathbf{B} / \mu_0)$ can itself be decomposed into two parts:

$$\begin{aligned} \mathbf{f} &= \mathbf{j} \times \mathbf{B} \\ &= (\nabla \times \mathbf{B} / \mu_0) \times \mathbf{B} = -\nabla(B^2 / 2\mu_0) + (\mathbf{B}\nabla)\mathbf{B} / \mu_0 \end{aligned} \qquad (4)$$

The first term on the right hand side, being a gradient, is the 'magnetic pressure', which can be incorporated into a modified pressure function:

$$p_m = p + B^2 / 2\mu_0 - \chi B^2 / 2\mu_0 \qquad (5)$$

That also includes the force on the magnetic material. For a diamagnetic, $\chi < 0$, the magnetic contribution gives an additional 'compression' to the liquid droplet. However unlike the induced current component, this magnetic force is not concentrated in the skin-layer. The magnetic pressure function is used to modify the free surface boundary condition for the diamagnetic part of the force. The AC field induced part is always solved explicitly within the fluid volume to account for both the rotational and the gradient parts in (4).

2.2 Computing the Flowfield

To determine the flowfield within a levitated liquid mass, the numerical model solves the momentum and mass conservation equations (6), with the modified pressure term defined in (5), which will also include the effect of gravity:

$$\partial_t \mathbf{V} + (\mathbf{V} \cdot \nabla)\mathbf{V} = -\rho^{-1}\nabla P_{\mathrm{mod}} + \nu_e \nabla \cdot (\nabla \mathbf{V} + \nabla \mathbf{V}^T) + \rho^{-1}\mathbf{J} \times \mathbf{B} \cdot$$
$$\nabla \cdot \mathbf{V} = 0 \qquad (6)$$

Note, that ν_e in (6), represents the effective viscosity, which may contain the turbulent contribution. The boundary conditions for (6) at the free surface relate normal stress to the surface tension,

$$\mathbf{e_n} \cdot \Pi \cdot \mathbf{e_n} = \Gamma K, \qquad (7)$$

continuity, and the tangential stress conditions:

$$\nabla \cdot \mathbf{V} = 0, \quad \mathbf{e_n} \cdot \Pi \cdot \mathbf{e}_{\tau 1} = 0, \quad \mathbf{e_n} \cdot \Pi \cdot \mathbf{e}_{\tau 2} = 0 \qquad (8)$$

Where, $e_n, e_{\tau 1}, e_{\tau 2}$ are the unit vectors normal and tangential to the free surface, Π is the stress tensor and K is the surface curvature. The free surface shape $\mathbf{R}(\theta, t)$ is updated at each time step using the kinematic condition:

$$\partial_t \mathbf{R} \cdot \mathbf{e_n} = \mathbf{V} \cdot \mathbf{e_n} \qquad (9)$$

The magnetic field in a solenoid is modeled as a superposition of the magnetic field generated by axisymmetric coil filaments of finite cross-section (see **Fig. 1** as an example). The electromagnetic body force requires in general an additional equation to be solved for the electric potential (only in the 3D case). The equation for the electric potential is obtained from the charge conservation $\nabla \cdot \mathbf{J} = 0$. Taking the divergence of the electric current density, gives:

$$\nabla^2 \phi_E = \nabla \cdot (\mathbf{V} \times \mathbf{B}) \qquad (10)$$

This equation is solved subject to the condition at the instantaneous drop surface: $\mathbf{J} \cdot \mathbf{e_n} = 0$.

In most situations, the flowfield in the droplet becomes turbulent. For this reason, a turbulence model needs to be used. The 'k-ω' turbulence model, where k is the kinetic energy of turbulence and ω the turbulent frequency, modified to include the effects of DC magnetic field damping[17] is used,

$$\partial_t k + \mathbf{v} \cdot \nabla k = \nabla \cdot [(\nu + \sigma_k \nu_T)\nabla k] + G - \beta^* \omega k - 2\alpha_m k \sigma B^2 / \rho$$
$$\partial_t \omega + \mathbf{v} \cdot \nabla \omega = \nabla \cdot [(\nu + \sigma_\omega \nu_T)\nabla \omega] + \alpha G \omega / k - \beta \omega^2 - \alpha_m \omega \sigma B^2 / \rho \qquad (11)$$

with 'no flux' boundary conditions prescribed at the surface:

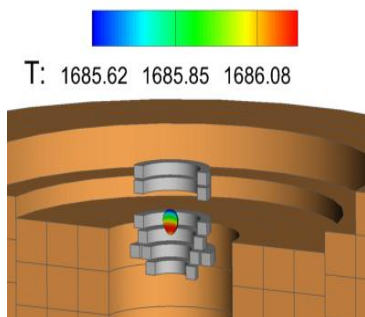$$\partial_n k = 0, \quad \partial_n \omega = 0. \qquad (12)$$

Fig.1 A typical terrestrial arrangement used for the measurement of thermal conductivity in a liquid droplet, with an AC levitating coil positioned in the core of a solenoid DC magnet

In addition to the stirring and levitation forces, the induced current in the droplet generates heat, through the Joule term $q_J = J^2/\sigma$ (W/m^3). Heat transfer within the droplet is then characterized by the transport equation

$$\rho C_p (\partial_t T + \mathbf{V} \cdot \nabla T) = \nabla \cdot (\rho C_p \alpha_e \nabla T) + q_J + q_L \qquad (13)$$

The last term in (14), represents the latent heat. Heat is lost by radiation at the surface, as given by the boundary condition:

$$-\boldsymbol{n} \cdot (-k\nabla T) = \varepsilon \sigma_T (T_{amb}^4 - T^4) \qquad (14)$$

Where, σ_T is the Stefan-Boltzmann constant.

3. Example Simulations

3.1 Silicon Droplet in AC/DC Field

Starting with simulations performed under terrestrial conditions, the following section contains the results of computations for an axisymmetric molten silicon droplet (diamagnetic, electrically conducting). It reproduces the method reported in Tsukada et al. [13], which uses periodic laser heating to determine the thermal conductivity of an electromagnetically levitated droplet. The static DC field is used to suppress convection. **Figure 1** shows the model setup and **Fig. 2**, the instantaneous spectral collocation mesh used within the droplet. Dynamic spectral computations with the code SPHINX were compared against experimental data from[9,13] and in static situations against the commercial code COMSOL[18]. Since under the conditions of the experiment the droplet tends to oscillate along the vertical axis, we examine the sensitivity of the measured temperatures to displacement within the levitating coil. In this situation, the levitating coil also provides the heat required to maintain the droplet in a liquid state. The difference in stability as the gravity is removed is also examined.

Tsukada et al.[13] report results on temperature/fluid flow in the droplet for the case when the laser is absent. Assuming the same geometry, material properties and operating conditions, these results have been closely replicated with COMSOL.
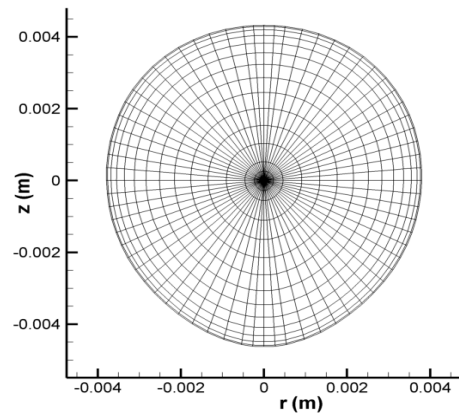

Fig. 2 The mesh used in spectral simulations

The solution in **Fig. 3** shows a scalar plot of |**B**| and streamlines of magnetic flux. The current is confined to a thin skin and concentrates on the inner surfaces of the coils where the contours are tightly bunched. The highest values of |**B**| are found in the space enclosed by the bottom coil turn which has the smallest radius and leads to higher flux confinement. The top two turns of the coil have the opposite sign to the lower set since they enclose flux which is oppositely directed.
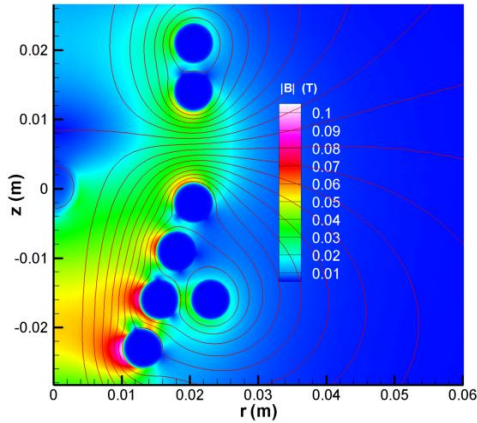

Fig. 3 COMSOL model of electromagnetic levitator (f=200 kHz, I_{peak} = 375A)
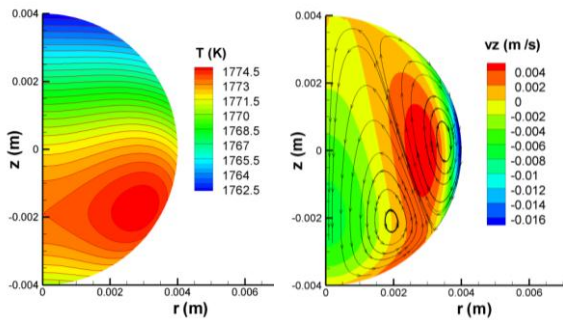
Fig. 4 Computed scalar plots of temperature T and velocity component V_z, in a spherical droplet.
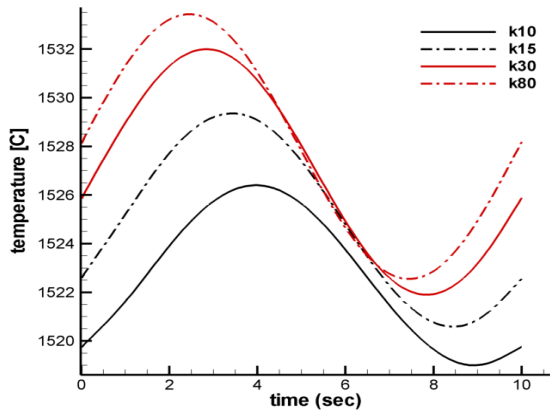
Figure 4 shows scalar plots of v_z and temperature in the droplet when a uniform DC magnetic field of 4T is applied. The results closely match, qualitatively and quantitatively, those produced in[13]. Two circulating vortices are present and the highest temperatures form a circular plateau in the lower half of the droplet.

Tsukada et al.[13] report the variation in phase shift according to the choice of thermal conductivity when the laser frequency is 0.1 Hz. These results have been reproduced here, and **Fig. 5 (left)** shows the temperature modulation state at the bottom of the droplet over one cycle of laser heating with frequency f_{laser}=0.1Hz for various thermal conductivities $k=\alpha\rho C_p$. **Figure 5 (right)** shows how the phase shift between these waveforms and that of the laser (taken as the reference) depends on the choice of k. The phase shift becomes less as the value of k is increased.

Figure 6 shows how the (time-averaged) axial force on the droplet $\int \mathrm{Re}(B_r J_\phi^*)/2\, dV - mg$ varies according to its z-position on the symmetry axis of the coils, with and without the influence of gravity. The zero-crossings of the curves indicate positions where the force is balanced. In earthbound conditions there is one stable and one unstable equilibrium, whereas in zero-gravity there is one stable and two unstable equilibria. The equilibria are indicated by the hollow (stable) and solid (unstable) circles. The results in **Fig. 6** can be used to generate phase-space portrait diagrams in (z,v_z) space describing the motion when the droplet is displaced off its equilibrium, by fitting a spline through the graphs and applying a standard ode solver to evolve the following pair of differential equations forward and backwards in time:

$$\frac{dV_z}{dt} = \frac{F_z(z)}{m} - g, \quad \frac{dz}{dt} = V_z$$
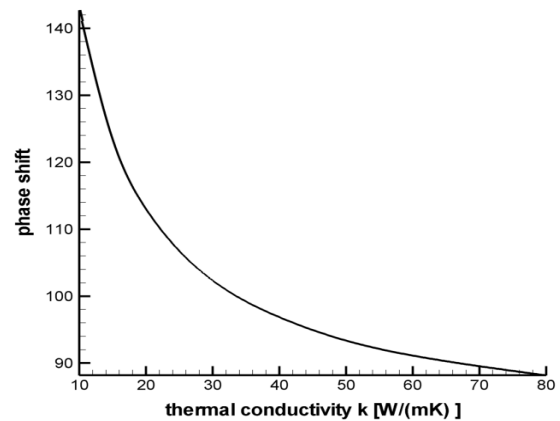

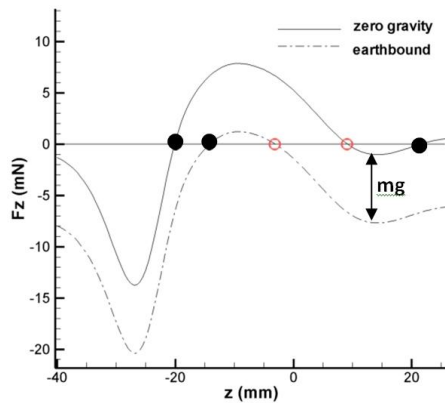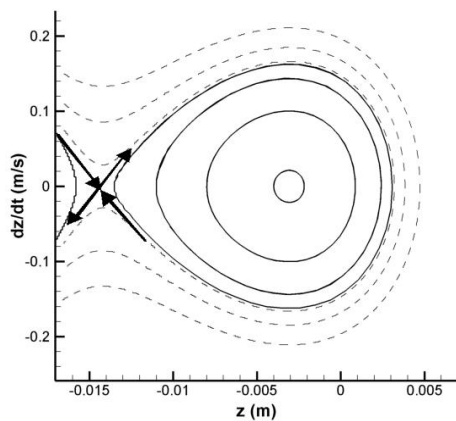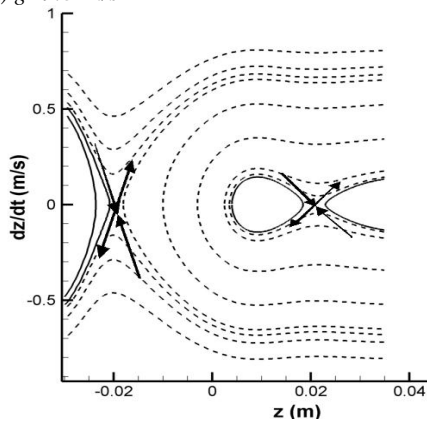**Fig. 5** Temperature modulation state (left) and phase shift as a function of k (right) when f_{laser}=0.1Hz

Fig. 6 The axial force on the droplet as a function of *z*.

(a) g=9.81m/s²

(b) g=0m/s²

Fig. 7 Phase space portraits in earth-bound (top) and zero gravity (bottom) conditions

Phase space portraits for earthbound and zero gravity conditions are given in **Fig. 7**. The closed curves indicate oscillatory motion around the stable equilibria, while the dotted curves represent "fly-by" trajectories where the droplet is temporarily caught in the field of the coils but does not remain permanently bound. The unstable equilibria are associated with hyperbolic fixed points whose stable and unstable manifolds are indicated by the arrows.

The unstable equilibria in zero-gravity are of relevance because, irrespective of the presence or absence of gravity, it is at these positions that Joule heating in the droplet approaches local maxima and where strong coupling occurs. The gradient of the heating curve at the earthbound stable equilibrium is quite high – found to be approximately 8 W/mm - which would suggest that even small amplitude oscillations could cause significant fluctuation in the temperature, highlighting the importance of eliminating axial motion when measuring the phase shift in the temperature oscillation. Since any droplet displacement also affects the impedance of the levitating coil, variations in power would also affect the measurements[4].

The COMSOL simulations presented in the stability analysis are for a rigid, spherical droplet and the flowfield was assumed laminar due to the presence of a DC field. However, true dynamic simulations are needed to account for changes in the shape of the droplet due to the time-varying forces acting on it, and turbulence must be included as it will modify the internal flow and temperature distribution. The spectral code SPHINX was used for this purpose.

The plots of velocity and temperature (without laser heating or DC field) in **Fig. 8** were obtained using a peak current of 530A in the excitation coil. Without the DC magnetic field, intense turbulent flow develops in the interior of the droplet.

Compared to the plot of temperature in **Fig. 4**,where the flow was laminar and assumed damped by the strong DC magnetic field, turbulence enhances the effective thermal diffusion and reduces the temperature variation throughout the droplet from 12° to just over 3°. The average temperature is about 85°C lower, due to the adjustment in operating conditions that makes the deformed droplet rest higher in the field and so experiences lower levels of Joule heating. Fluid velocities of 0.1 m/s are realized, making a Reynolds number of the order 10^4. In this scenario, the droplet assumes the more realistic diamond shape with dimensions as indicated in **Fig. 8**.

Now consider what happens when the static magnetic field is gradually increased. At moderate field strengths when B_{dc}=1T, the flow intensity actually increases compared to the situation when B_{dc}=0 T. This is apparent from **Fig. 9** which shows large-scale circulation velocities up to 0.2 m/s. In this scenario the mean large-scale flow is readjusted in a pattern along the vertical DC magnetic field (compare **Figs. 8** and **9**), the turbulence is damped by the magnetic field and the effective viscosity reduced to a near- laminar value. Compared to **Fig. 8**, the temperature variation throughout the droplet has increased from 3° to 6° - presumably because the shift in the position of the vortices reduces convective heat transfer to the top of the droplet.
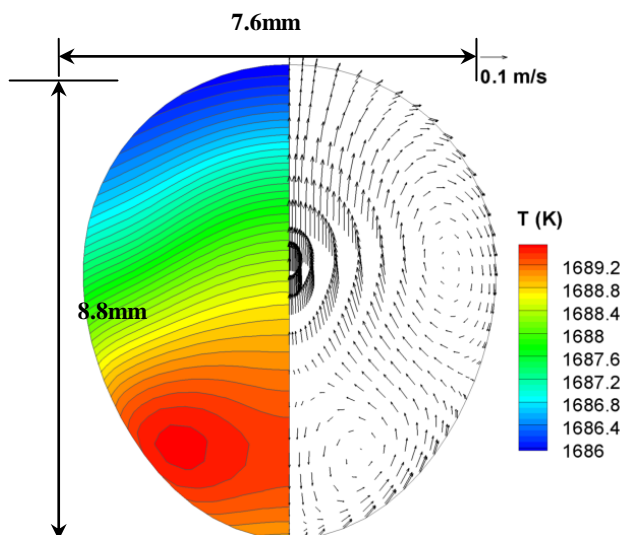
60   Int. J. Microgravity Sci. Appl. Vol. 30 No. 1 2013
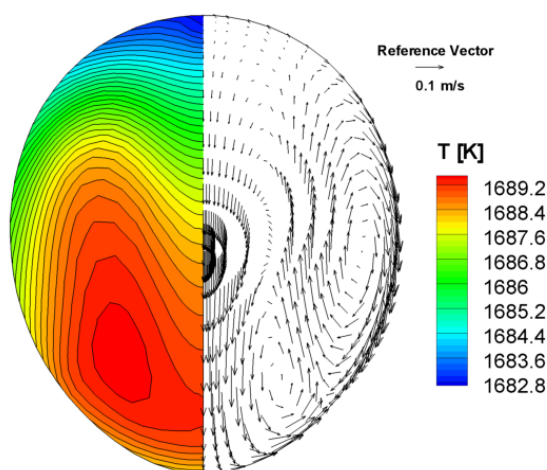
60

7.6mm

8.8mm

0.1 m/s

T (K)

1689.2
1688.8
1688.4
1688
1687.6
1687.2
1686.8
1686.4
1686

Fig. 8 Temperature and velocity, no DC field

Reference Vector
0.1 m/s

T [K]

1689.2
1688.4
1687.6
1686.8
1686
1685.2
1684.4
1683.6
1682.8

Fig. 9 Velocity/temperature field when B_{dc}= 1 T.

Reference Vector
0.01 m/s

T [K]

1692
1691
1690
1689
1688
1687
1686
1685
1684
1683

Thermo-Capillary
Convection
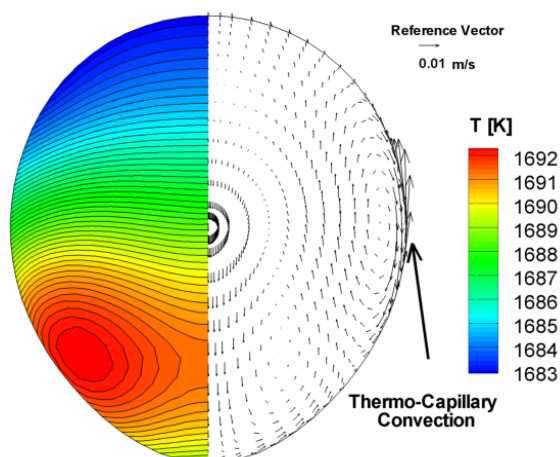
Fig. 10 Velocity/temperature field when Bdc= 5 T

Increasing further the strength of the DC field suppresses more effectively the radial component of velocity and generally decreases convection. **Figure 10** shows the velocity and temperature field at B_{dc}=5T where conditions approaching laminar flow and heat transfer are achieved. Thermo-capillary effects become noticeable on the surface of the droplet which are not easily damped by the action of the vertical DC field lines. The temperature variation throughout the droplet is now 11° and velocities of around 0.006 m/s occur on the symmetry axis. This compares well with the earlier results in **Fig. 5** and suggests that, while the average temperature in the droplet is lower due to the adjustment in shape and position, the spatial distribution of T is similar to that obtained for a spherical droplet.

3.2 A Copper Sphere in the MSL-EML Levitator

In this case the proposed design for the MSL-EML device is evaluated for microgravity operation. It features two 'pancake' coils using a dual frequency supply, one to provide heating and the other to stabilize the suspended charge in flight (**Fig. 11**) .

Each turn of the top coil carries AC current at a frequency of 146 kHz, I_{eff} = 139 A ('+I' current at the top and '-I' at the bottom) – *the positioning field*. The same coil is also carrying AC current at a frequency of 370 kHz, I_{eff} = 0 - 150A all in the same direction – *the heating field*. Initially the sphere is solid at room temperature, heats due to the action of the two fields melting after 10-11s and the heating current is then reduced to I_{eff} = 50A.

To calculate the stability of this system, the solid copper sphere was displaced first vertically along the coil axis, and then radially, with the positioning field on, but no heating field. The restoring force was calculated and the results given in **Figs. 12** and **13**. There is good correspondence between laboratory measurements[19] and the COMSOL simulations for this configuration. In both directions the system is stable with displacements up to 5mm in either direction, but beyond these limits it becomes unstable.
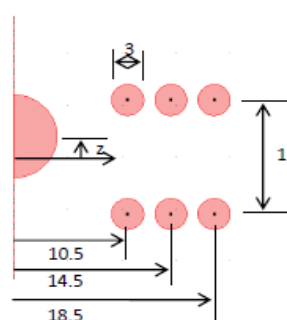
3

z

11

10.5

14.5

18.5

Fig. 11 Schematic diagram of the MSL-EML levitator consisting of one pair of 3-turn pancake coils, containing a 4mm suspended copper sphere (dimensions in mm)
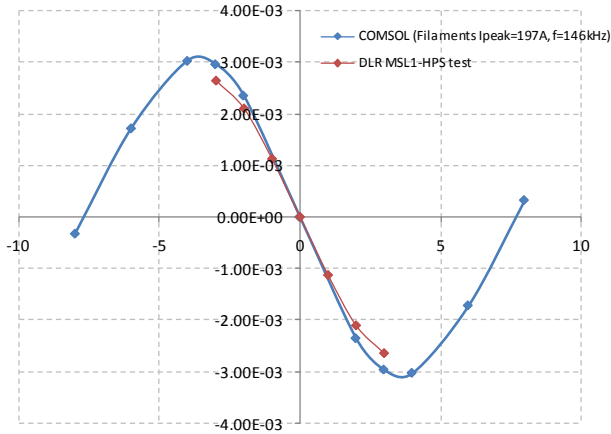
Fig. 12 Computed vertical force on a copper sphere as a function of vertical displacement from mid-position when a lifting-coil current of I_{peak}=197 A, f=146 kHz is applied – experimental results by Lohofer[19]
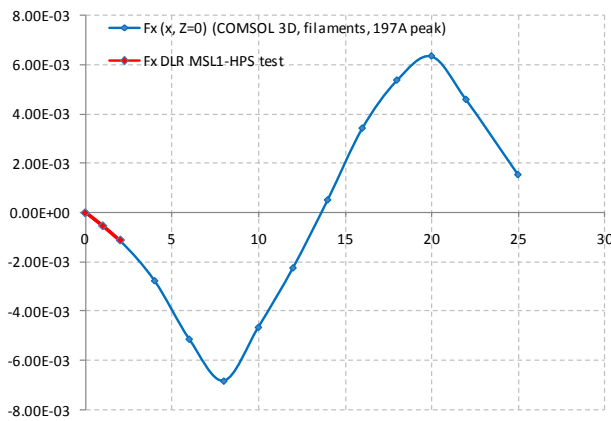

Fig. 13 Computed radial restoring force on copper sphere as a function of radial displacement from coil axis when a lifting-coil current of I_{peak}=197 A, f=146 kHz is applied – experimental results Lohöfer [19]

However, in practice the heating and positioning currents act together, at least until the sphere has reached the required temperature and once the sphere has melted, it no longer remains perfectly spherical. Since the heating current flows uni-directionally in both coils, what is the effect on stability?

To answer these questions, the problem was simulated dynamically using the spectral code SPHINX. **Figure 14** first, shows the resulting flow vectors and temperature contours in the liquid copper sphere with both positioning and heating fields on. The strong convection, coupled with the excellent thermal conductivity of copper, keep the temperature almost uniform, although the influence of the heating field can still be seen around the droplet equator. The flow exhibits toroidal vortices that '*pump*' the fluid towards the poles, then returning as a fast stream within the thin skin layers placed directly facing the coils. The shape of the droplet becomes elliptic, stretched slightly along the axis.

In contrast, when the heating field is switched off, the spherical shape returns, but the flowfield (**Fig.15**) looks
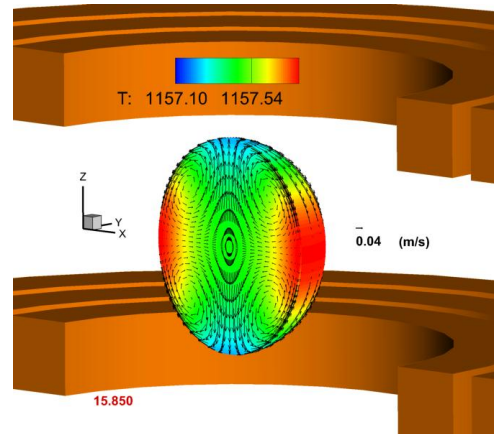

Fig. 14 Steady-state conditions, B=0T, f_{heat} =360kHz, I_{heat}= 50A, f_{pos} =146kHz, I_{pos}= 139A
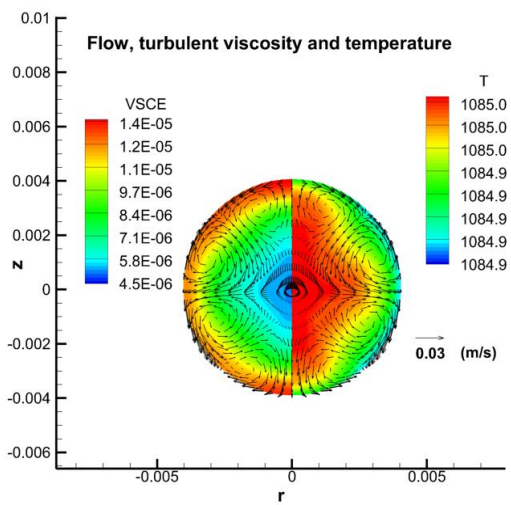

Fig.15 Flow field and contours of turbulent viscosity (left), contours of temperature (right) – heating field off, B=0T

completely different. The number of toroidal vortices has now doubled, with strong jets flowing towards the center from mid-latitude positions and returning to the surface along the poles and the equatorial plane. The temperature is still fairly uniform, although the effects of radiation cooling down slightly the surface of the sphere are now apparent. There is some turbulence also generated along the surface due to shear in the skin layers; however the value of the effective viscosity remains quite low – encouraging for viscosity measurements.

When a DC field of 1T is superimposed onto the positioning field (**Fig.16**), then the flow is damped (note the scale of vectors is reduced from 0.03m/s to 0.015m/s), with only the equatorial vortices still maintaining some strength. At the same time, the viscosity drops to the laminar value, and the temperature in the droplet remains uniform to within 0.1°C. Increasing the DC field even further to 5T (**Fig. 17**) -the value recommended above for terrestrial measurements, leads to a total suppression of convection within the droplet, although fast jets appear along the surface in regions of high temperature gradient, due to thermo-capillary action.
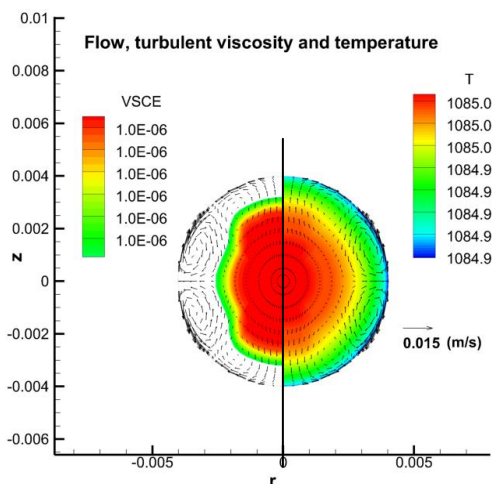
Fig. 16 Flow field and contours of turbulent viscosity (left), contours of temperature (right), with DC field added at B=1T and heating field off.

Fig. 17 Time history of the top polar point of the droplet as the DC field increases from 0T to 5T

It is not just the internal flow that is affected by the DC magnetic field, but also the motion of the droplet center of mass within the coils and its surface oscillations. Plotting the top polar point position against time, we can observe in **Fig. 18** that as the magnetic field strength increases from 0T to 1T, the motion of the droplet surface is rapidly damped in microgravity.

4. Conclusions

This brief review demonstrates the use of modeling to identify the role of static magnetic fields in the EM levitation of metallic liquid droplet, both in microgravity and under terrestrial conditions. It clear that an imposed DC field has an immediate effect on internal flow structure. At low level (0-1T) it is turbulence that is suppressed first, together with large vortical structures. As the field strength increases, the flow is damped altogether and the droplet oscillates as a solid body. A field of 5T was needed to suppress surface oscillations in full gravity, but 1T was sufficient in microgravity. In microgravity
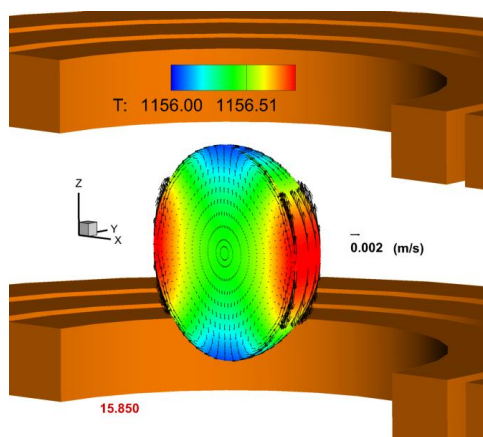

Fig. 18 Flow field and contours of turbulent viscosity (left), contours of temperature (right), at g=0, with DC field added at B=1T and heating field off.
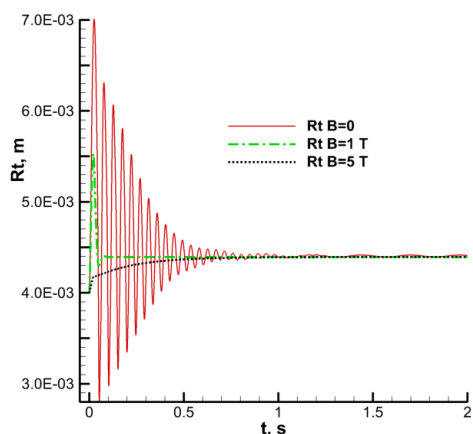
the droplet remains nearly spherical, whilst under full gravity it becomes egg-shaped due to the higher levitation force needed.

References

1) E. Okress, D. Wroughton, G. Comenetz, P. Brace and J. Kelly: J. Appl. Phys., **23**, 545 (1952)
2) I. Egry, G. Lohofer, I. Seyhan, S. Schneider and B. Feuerbacher: Int. J. Thermophys. **20** (4) 1005 (1999)
3) D. L. Cummings and D. A. Blackburn: J. Fluid Mech. **224** 395 (1991)
4) V. Bojarevics, K. Pericleous, A. Roy, S. Easter: Minerals, Metals and Materials Soc./AIME, Warrendale pp 14-18 (2010)
5) V. Bojarevics, K. Pericleous (2003), ISIJ International, 43, 6, 890-898
6) V. Bojarevics, R.A. Harding, K. Pericleous and M. Wickins: Metall. Mat. Trans. B, **35B**, 785 (2004)
7) V. Bojarevics, A. Roy, K.A. Pericleous: COMPEL- The Int J. Comp. Math. in Electrical Electronic Eng., **30** (5) 1455 (2011)
8) H. Fecht, R. Wunderlich, E. Ricci, J. Etay, I. Egry, S. Seetharaman and L. Battezzati: J. Jpn. Soc. Microgravity Appl. **27** (4) (2010)
9) H. Kobatake, H. Fukuyama, I. Minato, T. Tsukada and S. Avaji : Appl.Phys. Lett. **90** (2007)
10) V. Bojarevics, S. Easter, A. Roy and K.A. Pericleous: Proc. Int. Symp. Liquid Metal Processing and Casting, Santa Fe, TMS, ed- P.D. Lee et al., 319 (2009)
11) J. Etay, P. Schetelat, B. Bardet, J. Priede, V. Bojarevics and K. A. Pericleous: High Temp. Mat. and Processes, **27** (6) 439 (2008)
12) J. Priede: J. Fluid Mech. **671** 399 (2010)
13) T. Tsukada, H. Fukuyama and H. Kobatake: Int. J. Heat Mass Transfer, **50**, 3054 (2007)
14) V. Bojarevics and K. Pericleous: MHD Historical Evolution and Trends, in: Fluid Mechanics and Its Applications , Ed-s: S. Molokov et al. Springer, **80**, 357, (2007)
15) L.D. Landau and E.M. Lifshitz: Electrodynamics of Continuous Media. Pergamon (1984)
16) W. R. Smythe: Static and Dynamic Electricity, McGraw-Hill, London (1950)
17) O. Widlund: Ph.D. Thesis, Royal Inst. Techn., Stockholm, Sweden, ISSN 0348-467X, 2000.
18) COMSOL multiphysics (v. 3.5) www.comsol.com
19) V. Bojarevics, A.Roy, G. Lohöfer, K.A. Pericleous and A.Seidel: To appear, Proc. TMS annual meeting   (2013)